

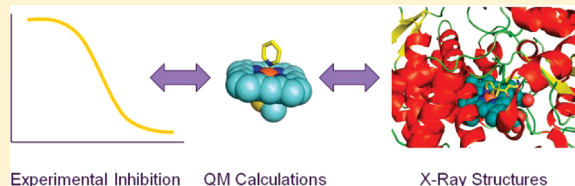
Quantitatively Interpreted Enhanced Inhibition of Cytochrome P450s by Heteroaromatic Rings Containing Nitrogen

Andrew G. Leach* and Nathan J. Kidley

AstraZeneca Pharmaceuticals, Mereside, Alderley Park, Macclesfield, Cheshire, SK10 4TG, United Kingdom

 Supporting Information

ABSTRACT: It has been known for a long time that certain substructures bind to the heme iron in cytochromes P450. Detection of spectroscopic changes and crystal structures of protein ligand complexes have provided qualitative evidence, including for aromatic nitrogen-containing ligands. Compounds containing these same substructures are more likely to inhibit cytochrome P450s than expected due to lipophilicity. These two sets of observations are not easily linked by experiment, because binding to the iron atom alone is not readily measured. Quantum mechanical (density functional) calculations of binding energies for a number of different aromatic heterocycles to heme iron in a range of oxidation and spin states can provide a quantitative link between the observed structures and the biochemical inhibition that is measured. The studies reported here for a set of heteroaromatic rings containing nitrogen begin with quantum mechanical calculations which provide geometries and binding energies. Subsequently, AstraZeneca's database of cytochrome P450 inhibition assays has been searched to find data that are relevant to the same set of heteroaromatic compounds. These data have been analyzed in a number of fashions to account for both the narrow dynamic range of the assays and the lipophilicity dependence of this kind of inhibition. Finally, crystal structures have provided experimental geometric information. Taken together these different sources suggest that binding to the metal in our inhibition assays is dominated by Fe^{III} in its doublet state, most likely occurring when the iron is pentavalent. Computed binding energies to this state contrast with the hydrogen-bond acceptor ability and basicity of the compounds, neither of which are able to correctly account for the effect of the particular environment in which the iron is found. This highlights the value of modeling biochemical events as closely as can be computationally afforded. The computational protocol devised was used to make predictions about a set of as yet unknown heteroaromatic compounds suggested by Pitt et al.



INTRODUCTION

A number of publications in recent years have highlighted the advantages of lower lipophilicity compounds. They are likely to have better pharmacokinetic and safety profiles among other benefits.^{1–3} Many of these same publications highlight the complementary role of molecular weight and the interplay between molecular weight and lipophilicity; lower molecular weight compounds tend to be more likely to be successful drugs.^{1,4} One simple strategy to lower the lipophilicity of compounds without simultaneously increasing their molecular weight is to replace aromatic CH groups with aromatic nitrogens, for instance, transforming phenyl groups to pyridines. The key risk with this strategy is that the nitrogen will not be tolerated by the target of interest, but a further complication is that some of these aromatic nitrogen atoms have been associated with enhanced inhibition of cytochrome P450s.

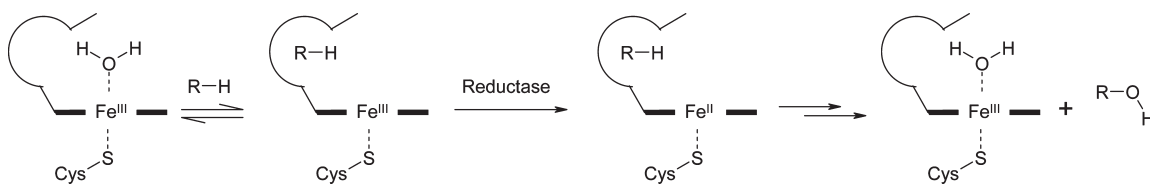
Cytochrome P450s (CYPs) are a major component of the metabolic process and are particularly concentrated in the liver, although they are present in many parts of the body.^{5,6} Xenobiotics are generally absorbed from the gastrointestinal (GI) tract into the hepatic portal vein which delivers them to the liver. Here, the CYPs dominate the so-called first pass metabolism to which the compounds are exposed. These enzymes therefore have a profound effect upon the amount of a compound that enters

circulation in the plasma (its pharmacokinetics) and can transform any given compound into a host of metabolites, some of which may be harmful.^{5,7} Hence, both the efficacy and tolerability of a compound are affected by CYPs. These are two of the factors most likely to cause a compound to fail in the clinic, or worse on the market.⁸ It is because of this central role in controlling the rate and nature of the metabolism of drug compounds that inhibition of the cytochromes P450 by other drug compounds is a concern.^{9–11} If the metabolism of one drug is reduced by the presence of another, then that drug's exposure levels in the plasma can go from safe and efficacious levels to higher toxic levels. Most drug compounds whose clearance is dominated by cytochrome P450 mediated oxidation are processed by one of five isoforms: 1A2, 2C9, 2C19, 2D6, and 3A4.^{12,13} Inhibition of any of these five in particular is likely to lead to concerns about comedication with other compounds.

The risk of these drug–drug interactions posed by inhibition of cytochrome P450 has meant that substantial efforts have been made to develop screening assays. It has been shown that such in vitro assays can provide a route map to establishing safety in the clinic.¹⁴ Fundamental biochemical and biophysical studies have

Received: February 1, 2011

Published: May 04, 2011

Scheme 1. Proposed Catalytic Cycle of the Cytochromes P450 Excluding Species in which O₂-Derived Ligands Are Bound^a

^a R—H is the substrate molecule that is oxidized to ROH. The bold lines represent the porphyrin-based heme ligand, and the thinner curved section represents the remainder of the protein binding site.

also been motivated by a desire to tackle these risks in a more systematic fashion. These have established that the oxidation by the CYPs is performed by an iron-based heme catalyst in an enzyme active site where four coordination sites on iron are filled by the porphyrin of the heme, the fifth is filled by a cysteine anion, and the sixth is exchangeable.^{5,15} The details of the catalytic process by which oxidation happens remain the subject of fertile research.^{16,17} It is usually proposed that the resting state involves an Fe^{III} atom with water bound (Scheme 1). Subsequently, substrate binding initiates a reduction to an Fe^{II} species by reductases. This can then bind oxygen which can go on to cause the formation of activated, oxidizing species which will transform the substrate. Spectroscopic studies have been performed on these enzymes, indeed their very name refers to a distinctive portion of their UV spectrum.¹⁸ Such studies have enabled different ligands to be categorized as types I and II, according to the spectroscopic changes induced; it is inferred that type I ligands do not bind to the metal directly and type II do.¹⁹ The crystallographically deduced structures of these enzymes were originally of bacterial varieties which are generally soluble.^{20,21} More recently, the structures of the human isoforms mentioned above have been obtained, with the exception of 2C19.^{22–26} These structures have enabled the creation of a number of homology models, and docking studies have used these and the original structures.^{27–34} A key observation from the structural work is that the proteins tend to have a highly flexible active site.²⁶ This is consistent with their broad substrate and inhibitor specificity. One consequence of this flexibility and the generally hydrophobic nature of the binding sites is that inhibition tends to show a dependence upon lipophilicity.^{35–37} A number of attempts to model CYP inhibition using quantitative structure–activity relationship (QSAR)-based methods have shown logP or logD to influence the degree of binding.³⁸ This suggests that analyzing the binding of compounds to CYPs should take this nonspecific binding into account if trying to dissect out the contribution of direct (covalent) interactions between the iron and the ligand.

Alongside the experimental and QSAR studies, a parallel work employing quantum mechanical methods has been performed. In particular, Shaik and Thiel have published an extensive series of papers detailing different aspects of the reactivity of the heme in different liganded, oxidation, and spin states. They have proposed that a number of spin states for most of the species involved in the reaction contribute to the perplexing experimental observations.^{15–17,39–41} The Fe^{III} can be in doublet, quartet, or sextet spin states and Fe^{II} in singlet, triplet, or quintet states. Transitions between spin states are formally forbidden, and therefore it is possible for higher energy spin states to be kinetically trapped and so participate in the chemistry of these enzymes. More recently, de Visser et al. have described a binding

mode for a number of aromatic nitrogen-containing “azoles”, focusing on the process by which these ligands approach the water-bound heme and displace the water.⁴²

Here we report a series of studies which taken together shed light on the ability of compounds containing an aromatic nitrogen atom to inhibit cytochrome P450s. The approach could serve as a model for how such studies could be performed for other metal-chelating group types and other metal-containing binding site types. The first results we present are quantum mechanical calculations on complexes of a set of model ligands with an iron atom in a porphyrin to mimic the heme and with SMe to mimic the active site cysteine. In these calculations, iron is present as Fe^{II} and Fe^{III}, and the highest and lowest spin states of both are examined. The second set of results are from data mining of the AstraZeneca database to study how compounds containing particular substructures behave and to identify those compounds that show an enhanced propensity to inhibit CYPs. The third source of information is crystal structures of CYP–ligand complexes, focusing on those compounds containing a relevant aromatic nitrogen atom. Taken together these three sets of information support the enhanced binding of particular ligand types to iron as a rationale for their enhanced inhibition in relevant assays. Furthermore, they suggest that in such assays the state of iron that provides the best concordance between calculations and experiment is the lowest energy, doublet state of Fe^{III}. This binding to iron contrasts with the more general hydrogen-bond acceptor ability of the rings due to the particular steric environment involved. Finally, this link has been exploited to make predictions about a set of heterocycles that were recently highlighted as being unknown but likely to be synthetically tractable.⁴³ Although substantial computational effort is involved in these characterizations, it is generally more satisfactory to model the biochemical events as closely as possible in order to generate the right answer for the right reasons, and a small number of relevant calculations can provide useful insight if thoughtfully planned.

RESULTS AND DISCUSSION

The first strand of study to link binding to iron in the heme of cytochrome P450 to inhibition, as observed in our assays, was to use quantum mechanics to derive energetic and geometrical predictions about the interaction between iron and a set of nitrogen-containing heteroaromatic ring types. The calculations employed the B3LYP functional with a 6-31G* basis set for most atoms and the lanl2dz basis set and core pseudopotential for iron.^{44–49} These calculations were performed in Gaussian03.⁵⁰ Single point calculations using a larger 6-31+G** basis set in combination with the B3LYP functional and the 6-31G* basis set with the M06 functional were performed in Gaussian09.^{51,52} The

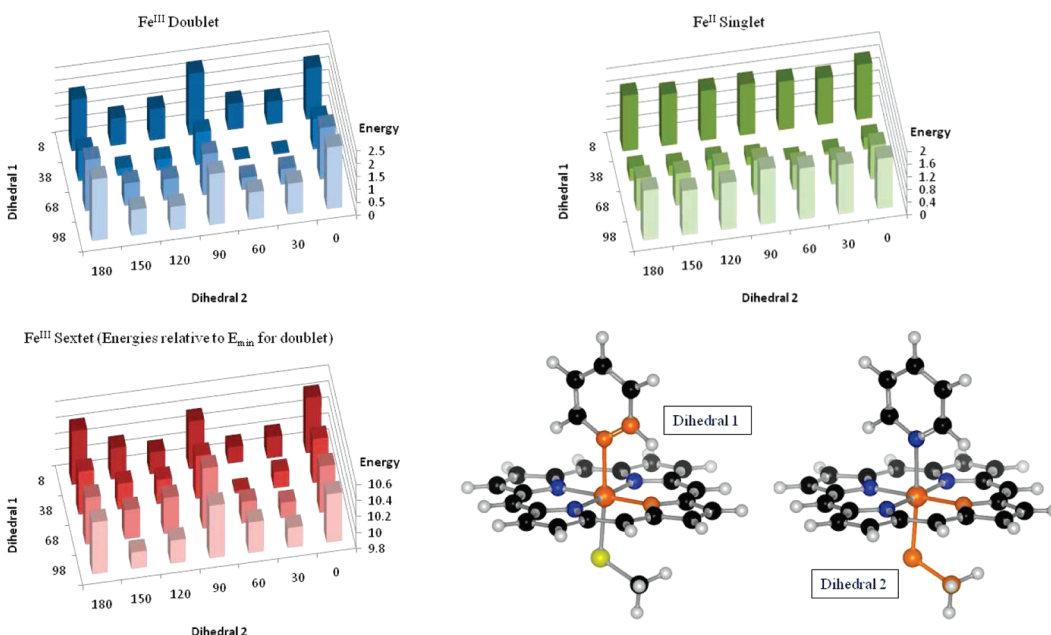


Figure 1. Column plots for the rotation of the SMe and pyridine about the N–Fe–S axis. The two dihedrals that form the x and y axes are highlighted in the chemical structures in orange. Energies in kcal/mol are indicated on the vertical axes. In top left are the energies for Fe^{III} in its doublet state relative to the lowest energy point (which ranges over 2.4 kcal/mol). In bottom left are energies for Fe^{III} in its sextet state, also relative to the lowest energy point on the surface for the doublet state (which ranges over 0.7 kcal/mol from 9.8 to 10.5 kcal/mol). In top right are energies for Fe^{II} in its singlet state (which range over 1.7 kcal/mol). Fe^{II} in its quintet state in all cases did not bind the ligand.

system studied employed MeS as a mimic for the cysteine that binds directly to iron as one of the apical ligands in the binding site (Scheme 1). An undecorated porphyrin is employed in place of the heme system. The first ligand studied was pyridine. Problems identifying a well-characterized minimum energy structure prompted a number of systematic scans of the geometry in which the pyridine and the SMe were rotated relative to the heme (Figure 1). Direct binding to iron at any stage of the process outlined in Scheme 1 would lead to enhanced inhibition, and so calculations focused on four states of iron: Fe^{III} in its high-spin sextet and low-spin doublet states and Fe^{II} in its high-spin quintet and low-spin singlet states.

Attempts to optimize structures in which ligands were bound to Fe^{II} in its quintet state resulted in the ligand dissociating from iron. This state was therefore not investigated any further, and only the low-spin Fe^{II} singlet was examined. Related behavior has been observed previously; even water dissociates from the high-spin complexes.⁵³ A feature of the surfaces shown in Figure 1 that is unusual is how flat they are. The whole space sampled for the Fe^{III} sextet is contained within less than 1 kcal/mol of energy variation, while for Fe^{II} in its singlet state, the energies cover a range of 1.7 kcal/mol and for Fe^{III} doublet state a range of 2.4 kcal/mol. Optimizations on such a flat surface are challenging, and the simple harmonic approximation used to derive the frequencies will be inadequate for such broad and shallow energy wells. This has consequences for any force field parametrization of these systems which must permit many orientations to be accessed at small energy penalties. It is interesting to note that the lowest position on each surface is the same and therefore is likely to be a preference driven principally by steric effects; the underlying electronic structure of the porphyrin and iron does not seem to exert a great deal of influence. The degree of corrugation on the contour plots might therefore depend upon the bond

lengths between iron and either sulfur or nitrogen. In the optimizations for Fe^{III} doublet the Fe–N distance varied in the range of 2.21–2.29 Å, for the sextet it varied in the range of 2.67–2.83 Å, and for Fe^{II} in the singlet state it varied in the range of 2.13–2.21 Å. Similarly, the Fe–S distance spanned the ranges of 2.23–2.24, 2.366–2.373, and 2.38–2.40 Å, respectively. These are consistent with the contour plots shown in Figure 1, as the variation of energy is the least for the sextet which has the longest Fe–N distances. The highest energy points are all reached by twists of dihedral 1; this corresponds to rotation about the Fe–N bond which is the shorter of the two distances for Fe^{III} doublet and Fe^{II} singlet. Subsequent studies employed the lowest energy conformation of the system which in all cases has the S–Me bond orthogonal to the plane of the aromatic ring of the ligand and has both the S–Me bond and aromatic plane sitting in the gaps between five-membered rings in the porphyrin ring. Similar contour plots as in Figure 1 were generated for many of the other ligands described below, but in all cases, the same minimum energy structure was found.

The studies were extended to a range of other heteroaromatic rings, detailed in Figure 2. For each, the structure of the ligand bound to iron through the nitrogen atom indicated in red was computed. The optimized structures of each complex are provided in the Supporting Information. Subsequently, the isolated ligands were optimized with B3LYP/6-31G*. Finally, two alternative reference states of the iron–porphyrin were selected: the pentavalent iron and the hexavalent with water bound (left- and right-hand equilibria in Scheme 2). The water-bound state was extracted from de Visser et al's studies for Fe^{III} ⁴² and was modified to obtain the equivalent for Fe^{II} .⁴² The geometries of all three reference complexes of water and the pentavalent complexes are also provided in Supporting Information.

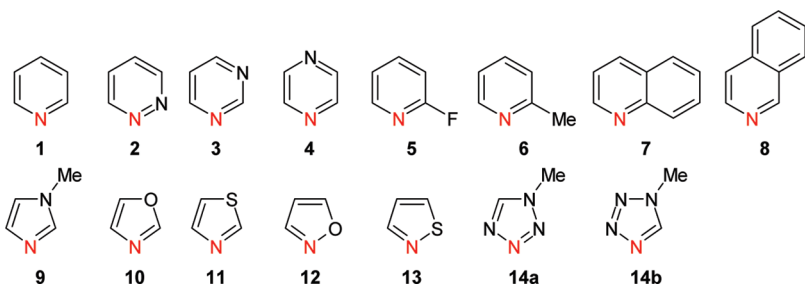
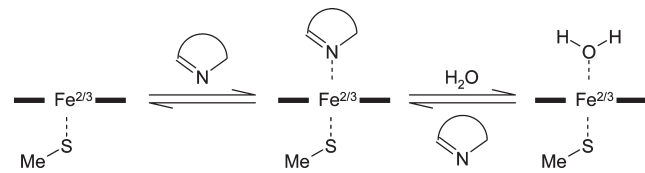


Figure 2. Ligands studied with quantum mechanics. The atom that is bound to iron in each case is indicated in red.

Scheme 2. Two Possible Ligand Exchange Processes for Which Energy Changes Have Been Computed Based on Density Functional Theory Calculations^a



^a The bold lines represent the porphyrin ligand.

The optimized geometries were subjected to frequency calculations to verify that they are minima. These calculations are problematic because of the flat surface for rotation and occasionally a low negative frequency was observed, which is noted. The frequency calculations on the various structures permitted the energy, enthalpy, and free energy changes for the processes outlined in general in Scheme 2 to be computed, and these are reported in the Supporting Information but are not discussed here due to the complications caused by the low negative frequencies. The electronic energy changes only are detailed in Table 1. The iron–nitrogen and iron–sulfur distances are also noted to help interpret the data. Single point energy evaluations were performed on all the structures obtained at the B3LYP/6-31+G** level in order to investigate the stability of the numbers with respect to the basis set size and at the M06/6-31G* level to investigate any potential effect of dispersion-based interactions. Both alternative levels gave good rank correlations with the B3LYP/6-31G* level, particularly for the Fe^{III} doublet. Ligands with ortho substituents or adjacent heteroatoms deviated from the correlation for Fe^{III} sextet and Fe^{II} singlet, neither provide better agreement with experimental observation as discussed below. M06/6-31G* predicts energies of complexation that are about 8–10 kcal/mol more favorable. The full complexation energies are provided in the Supporting Information.

Both of the ligand exchange processes shown in Scheme 2 were considered by using as reference states either the pentavalent iron complexes or the hexavalent complexes with water. This is equivalent to allowing the metal binding group to bind to any of the first three species shown in Scheme 1 as well as the notional Fe^{II} equivalent of the water-bound resting state. In all cases, replacing water with one of the ligands was computed to be uphill. If these absolute binding energies were correct, then enhanced binding to the ligands would be observed if they are binding to a pentavalent iron atom but not to the hexavalent water complex. It should be noted that the entropic consequences of displacing a tightly bound water might be significant. The computed binding energy (no vibrational corrections) for

water to Fe^{III} in its doublet state is 11.0 kcal/mol, in its sextet state 6.3 kcal/mol, and to Fe^{II} in its singlet state 11.2 kcal/mol. The fact that some of these ligand types do indeed demonstrate enhanced inhibition, as discussed below, is consistent with the experimental observation that the pentavalent state of iron is revealed by the enzyme at some point during its catalytic cycle, most likely concerted with substrate or inhibitor binding.⁵⁴

To understand whether the binding energies to the various states of iron show the same trends or suggest differences, the three sets of ΔE are plotted against one another in Figure 3. In the first panel, the energy of binding to the doublet and sextet states of Fe^{III} is plotted and reveals that for most ligands there is a broad correlation. Five- and six-membered aromatic rings behave similarly and are intermingled. The ligands which show a difference are those in which there are substituents next to the binding nitrogen atom. The 2-fluoro- and 2-methyl-substituted pyridine is away from the general trend in a way that suggests enhanced binding to the doublet or diminished binding to the sextet. The second two panels reveal that binding energies to Fe^{III} in its doublet state and Fe^{II} in its singlet state correspond fairly closely and that the binding to the sextet state is the binding energy that is different. This suggests that it is the steric influence of the substituents next to nitrogen in 2-fluoropyridine, 2-methylpyridine, and quinoline that causes these to be away from the line for the two states in which the Fe–N distance is short, whereas in the Fe^{III} sextet state where the distance is longer, this effect is weaker. The N-methylimidazole ligand also binds either surprisingly well to the Fe^{III} or surprisingly weakly to the Fe^{II}. In light of the experimental observations, it is likely that the latter is the case.

It is striking that the Fe–S distance varies little with the different ligands bound for any of the complexes. These distances are close to those observed in the unliganded state for Fe^{III} in its doublet state where the Fe–S distance is 2.21 Å. The distances in the complexed state are generally longer than in the pentavalent complex for Fe^{III} in its sextet state and for Fe^{II} in its singlet state, where in both cases it is 2.33 Å. The complexes with water also show that the Fe–S distance remains almost unchanged for Fe^{III} in the doublet state, where it is 2.22 Å. It is shorter in the complexes with the ligands in Figure 2 than in the complexes with water for Fe^{III} in its sextet state where it is 2.33 Å and for Fe^{II} in its singlet state where it is 2.37 Å. These observations of a variable optimal Fe–S distance for two states and much less variation for the third might be relevant to the mechanism of these enzymes in which the protein holds the cysteinyl sulfur and the heme in place. These distances are revisited below in the studies of the crystallographic structures. The other reported distance, between iron and the chelating nitrogen, is more variable in all states and broadly the higher the binding energy, the shorter the Fe–N

Table 1. Ligand Binding Energies to the Pentavalent Reference State and Iron–Nitrogen Distances for Complexes of Heteroaromatic Compounds with Different Oxidation and Spin States of Iron Porphyrins^a

ligand	Fe ^{III} doublet			Fe ^{III} sextet			Fe ^{II} singlet		
	ΔE	Fe–S	Fe–N	ΔE	Fe–S	Fe–N	ΔE	Fe–S	Fe–N
1 pyridine	-7.1	2.23	2.21	+0.8	2.37	2.71	-5.0	2.40	2.13
2 pyrazidine	-6.2	2.23	2.20	+1.6	2.37	2.69	-4.1	2.41	2.03
3 pyrimidine	-5.9	2.23	2.22	+1.3*	2.36	2.78	-6.5	2.40	2.11
4 pyrazine	-5.9	2.23	2.22	+1.2	2.36	2.79	-8.1	2.40	2.08
5 2-fluoropyridine	-2.4	2.23	2.42	+2.0	2.35	3.09	+0.6	2.38	2.29
6 2-methylpyridine	-0.5	2.23	2.65	+2.7*	2.34	3.82	+2.1	2.37	2.63
7 quinoline	+1.3	2.23	2.68	+4.0*	2.34	3.66	+3.4	2.36	2.65
8 isoquinoline	-5.0	2.23	2.21	+2.8	2.38	2.69	-3.3	2.40	2.12
9 N-methylimidazole	-8.7*	2.24	2.14	+0.2*	2.39	2.50	-3.1	2.41	2.11
10 oxazole	-6.6	2.23	2.17	+0.9	2.37	2.64	-5.4*	2.40	2.11
11 thiazole	-4.9	2.23	2.21	+2.1	2.36	2.74	-4.1	2.40	2.13
12 isoxazole	-3.7	2.22	2.20	+2.1	2.35	3.11	-2.4	2.40	2.05
13 isothiazole	-3.6*	2.22	2.22	+3.0*	2.36	2.84	-2.4	2.40	2.09
14a 1-methyltetrazole (3 linked to Fe)	-1.6	2.22	2.22	+4.3	2.36	2.95	+3.8	2.40	2.05
14b 1-methyltetrazole (4 linked to Fe)	-4.5	2.22	2.18	+2.5*	2.36	2.76	-2.4	2.40	2.09

^aValues marked with * involved a geometry computed to have a negative frequency which relates to a rotation of the aromatic nitrogen-containing ligand around the S–Fe–N axis and is an artifact of the calculations.

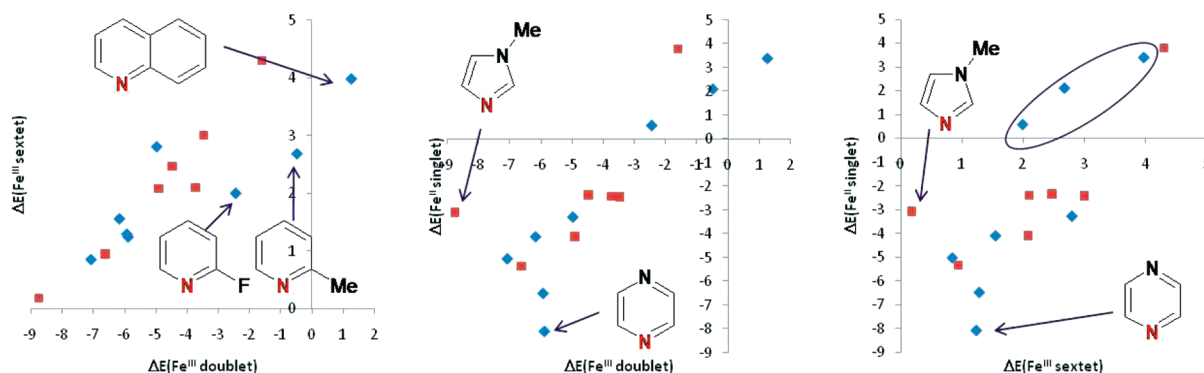


Figure 3. Binding energies for the ligands illustrated in Figure 2 to Fe^{III} in its sextet and doublet states and Fe^{II} in its singlet state correlated with one another. The ligands corresponding to some of the notable outliers are highlighted. These plots are of the data in columns 2, 5, and 8 of Table 1. Ligands in which the aromatic nitrogen atom is in a five-membered ring are colored in red, and those in a six-membered ring are colored in blue. The oval in the last plot highlights the points corresponding to 2-fluoro- and 2-methyl-substituted pyridines and quinoline.

distance. The Fe–N distance in each of the three states tends to correlate with that in the others, suggesting the same underlying effects determine this distance.

A subject of some interest and debate particularly with regards to the reactivity of the P450s is the splitting between the spin states of the various species. For Fe^{II} the presumed ground-state quintet does not appear to interact favorably with any of the ligands in Figure 2. For Fe^{III} the doublet is computed to be the ground state in all cases, and the differences between the sextet and doublet are given in Table 2. The corresponding gaps for the water-bound state and for the systems in which the iron is only pentacoordinate are also included to add context. Particularly tightly binding ligands, such as imidazole, widen the difference favoring the doublet, whereas weaker binding ligands, such as the ortho-substituted pyridines, reduce the gap between the two states but not quite to the degree achieved when the ligands dissociate completely. Even at the narrowest computed gap, the

difference is large enough that the sextet would not be expected to be significantly sampled at equilibrium. Experimental values support this qualitative observation, but it is overstated, and significant high-spin Fe^{III} can be observed and is often ascribed to the pentavalent state.⁵⁵

To link the computed energies to experimentally observed inhibition, the AstraZeneca P450 inhibition assays were mined. Whereas in the quantum mechanical calculations model ligands were studied, in examining the experimental data compounds containing analogous substructures have been studied. These are described as structural classes and were assigned to compounds using a set of SMARTS definitions that are given in the Supporting Information.⁵⁶ Essentially these correspond to the ring types illustrated in Figure 2 in which the positions adjacent to the nitrogen atom in red (or in the peri position in quinoline) are constrained to not have a substituent apart from for the 2-fluoropyridine and 2-methylpyridine groups. It should

Table 2. Gap between the Doublet and Sextet State in Ligand-Bound Species for Fe^{III}

ligand	doublet–sextet gap
pyridine	10.2
pyridazine	10.0
pyrimidine	9.5
pyrazine	9.4
2-fluoropyridine	6.7
2-methylpyridine	5.4
N-methylimidazole	11.2
oxazole	9.9
thiazole	9.3
isoxazole	8.1
isothiazole	8.8
1-methyltetrazole (3 linked to Fe)	8.2
1-methyltetrazole (4 linked to Fe)	9.2
quinoline	5.0
isoquinoline	10.0
water	7.0
none	2.3

also be noted that, whereas in the quantum mechanical calculations N-methylimidazole was used, there has been no control of whether the compounds classed as imidazoles or tetrazoles are N-substituted and therefore there could be an acidic NH available.

At the time that the data were extracted, 44 336 compounds had been studied in an assay against at least one of the five major isoforms. In these assays the ability of a compound to inhibit a cytochrome P450-mediated reaction is measured by monitoring the decrease in the rate of the oxidation of a standard substrate. More details are provided in the Experimental and Computational Procedures Section. Such assay data are frequently challenging to model due to the limited dynamic range that is accessed (typically they are unable to measure pIC₅₀ values that are less than ~5) and to the fact that most compounds are designed not to be inhibitors. In cases where the compound falls outside the range of an assay, the value that is returned within our database structure is the upper range of the assay; in most cases the upper range of the assay is a pIC₅₀ of 5, which accounts for 29% of all reported values. A complication of all analyses of P450 assay data is that more lipophilic compounds tend to be more potent inhibitors. To address this, lipophilicity corrected inhibition values are also derived. These will be described in detail for the analysis of the maximum pIC₅₀ values which follows. In this study, lipophilicity has been computed using the fragment-based clogP algorithm.^{57,58}

For each of the 44 336 compounds that are included in this study, the maximum pIC₅₀ reported against any of the five most common isoforms has been identified. This includes many compounds which do not cause inhibition inside the dynamic range of any of the assays. In such distributions, the mean is not a valid descriptor as many of these values are the upper range of the assay and not an actual measurement. Therefore for each type of structure, the 90th percentile in the distribution of the maximum values achieved for each structural class is extracted and reported in Table 3. This reveals that for the 2343 compounds containing a pyridine substructure, the top 10% all have a pIC₅₀ ≥ 7. This statistic has not been corrected for lipophilicity. The next value

computed is the number of compounds containing each substructure that are in the most potent 10% of all compounds measured. If this was a thorough sampling of structural diversity, then this value would indicate the probability of a compound containing a particular substructure of being a very potent inhibitor of at least one of the isoforms of cytochrome P450. The binomial distribution can be used to place 95% confidence intervals upon the proportion of potent compounds in the underlying population from the limited sample size upon which this analysis is based.⁵⁹ However, if the set of compounds assigned to each class happened to be unusually lipophilic that would confound this analysis. This is illustrated in Figure 4. The data set is binned into intervals of clogP that are 0.5 wide. Within each interval, the number of compounds that fall in the top 10% of potent inhibitors is plotted along with the number of compounds that fall in among the remaining 90% of compounds. Over this distribution is plotted the proportion of compounds in each bin that are in the top 10%, and this shows a very clear upward trend as clogP increases. Indeed, only 1.8% of compounds with a clogP of around 0 are in the top 10% of compounds, whereas more than 25% of those with a clogP > 6 fall in the top 10%. While the binned analysis in Figure 4 provides a useful illustration of the effect, the statistical analysis package JMP is able to fit a smoothed function through the continuum of points, and this can be used to compute a clogP based probability of being potent for each compound.⁶⁰ This function is $P(\text{clogP}) = 1/(1 + e^{3.84 - 0.44\text{clogP}})$ and similar values of the two variable coefficients are found for individual isoforms (see Supporting Information), with the exception of 1A2 which has an exponent of 2.81 – 0.18 clogP. From this equation, plotted in Figure 4, the mean probability of being potent (top 10%) according to clogP is then computed for each structural class along with the corresponding standard error. This is plotted against the observed number of compounds in each class that is actually found to fall in the top 10% in Figure 5. In this plot it is clear that five of the structural classes are found to be significantly more likely to be in the top 10% of inhibitors than predicted due to lipophilicity. The difference between the predicted and the observed proportions of each type in the potent group is recorded as excess probability in Table 3.

To analyze the continuous data, all measurements that are flagged as falling outside the dynamic range of the assay are excluded. The mean in-range pIC₅₀ is computed for each structural class, and these are reported in Table 3. Again, these values would be expected to be dependent upon lipophilicity. This is illustrated in Figure 6 where the observed pIC₅₀ values are plotted against the corresponding clogP values. There is a relatively weak dependence on clogP, but it is easy to remove this linear dependence by computing the residual between the observed pIC₅₀ for each compound and the value expected based upon its lipophilicity from the equation shown in Figure 6. The mean value of these residuals for each structural class is also reported in Table 3 along with the corresponding standard error.

The five structural classes that are distinct from the 1:1 line in Figure 5 are in bold text in Table 3. It is clear that across all measures these structural classes are more potent than the remaining classes. Thiazoles are slightly ambiguous being among the most potent group in the columns that do not involve lipophilicity corrections. In italic text, the 2-methylpyridine class is highlighted, which is also distinct from the 1:1 line but in the direction of being less potent inhibitors than expected.

Table 3. Summary Statistics for the Maximum Inhibition Values of Each Compound in Any of the Five Main CYP Isoforms Studied According to the Structural Classes to which They Belong^a

	N	pIC ₅₀ at 90th percentile	mean clogP based probability of being in top 10%		observed % in top 10% of all compounds		bottom end of 95% confidence interval		upper end of 95% confidence interval		excess Probability	N in range	mean pIC ₅₀ for in range values	SEM	mean residual away from clogP based line for in range values	SEM
			mean clogP based probability of being in top 10%	SEM	10% of all compounds	SEM	confidence interval	SEM	19.9	23.3						
pyridine	2343	7.00	9.2	0.1	21.6	1.1	0.2	5.8	5.8	-3.6	26	5.24	0.12	-0.24	0.10	
pyridazine	93	5.34	4.7	0.3	1.1											
pyrimidine	135	6.70	7.5	0.4	17.8	12.2	25.1	10.3	86	5.74	0.07	0.21	0.07			
pyrazine	283	6.42	6.9	0.2	9.2	6.3	13.1	2.3	207	5.61	0.04	0.13	0.04			
2-fluoropyridine	66	6.05	10.3	0.6	3.0	0.8	10.4	-7.3	47	5.41	0.08	-0.20	0.09			
2-methylpyridine	392	6.12	16.2	0.6	6.4	4.4	9.2	-9.8	247	5.50	0.04	-0.27	0.04			
quinoline	720	6.61	13.7	0.2	12.9	10.7	15.6	-0.8	533	5.64	0.02	-0.04	0.02			
isoquinoline	29	7.00	8.2	0.7	34.5	19.9	52.7	26.3	24	5.84	0.14	0.32	0.13			
imidazole	255	7.24	9.4	0.4	60.4	54.3	66.2	51.0	235	6.39	0.05	0.84	0.04			
oxazole	15	7.36	11.1	1.2	53.3	30.1	75.2	42.2	15	6.47	0.15	0.86	0.15			
thiazole	31	6.96	9.8	0.8	16.1	7.1	32.6	6.3	28	5.77	0.11	0.18	0.11			
isothiazole	6	5.70	6.5	2.0	0.0	0.0	39.0	-6.5	2	5.57	0.13	-0.10	0.07			
tetrazole	89	6.33	10.9	0.5	6.7	3.1	13.9	-4.2	66	5.38	0.07	-0.26	0.07			

^aThe pIC₅₀ at the 90th percentile is the value of pIC₅₀ above which 10% of the compounds in each structural class fall. The mean clogP based probability of being in the top 10% is the mean value of a function linking clogP to the likelihood of being in the top 10% of all compounds, and the next column is the standard error in that mean value. The following three columns are the actual percentage of compounds in each structural class that are measured to be in the top 10% of all compounds and the binomial based 95% confidence intervals on that percentage. The excess probability is the difference between columns 6 and 4. The number of compounds in each class that are measured to inhibit within the dynamic range of the assay are indicated in the N in range column. The mean pIC₅₀ for in range values is a mean of values that fall within the dynamic range of the assay, and in the following column the standard error in that mean. The mean residual in the following column is the mean of the vertical differences between the observed pIC₅₀ values and the line of best fit between clogP and pIC₅₀, and the final column is the standard error in that mean.

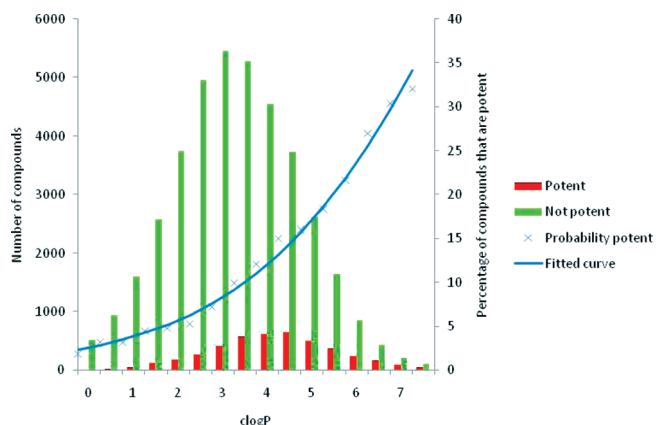


Figure 4. Number of compounds in particular ranges of clogP that are in the top 10% of most potent compounds across the 5 isoforms tested is shown. The number of compounds in the lowest 90% in terms of CYP activity is shown in green, while those in the top 10% are shown in red. The blue crosses indicate the ratio of the two groups. The blue line is the curve that is fitted through these points in order to assign a probability of being in the top 10% of individual compounds.

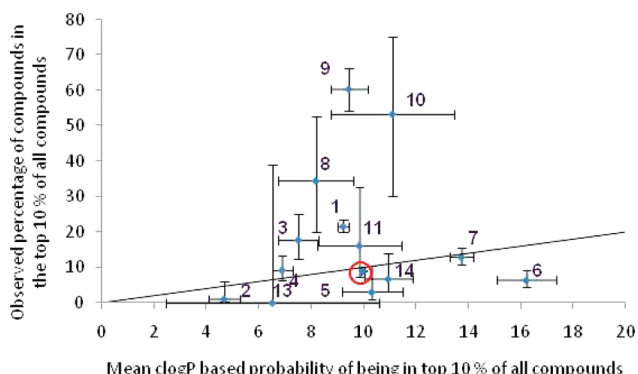


Figure 5. Observed frequency of compounds in the top 10% of all compounds in terms of the maximum pIC₅₀ they achieve against any of the five main isoforms of P450 plotted against the frequency that would be expected based on the clogP of the compounds in each structural class. The x-error bars are two standard errors in the mean of the distribution of clogP based predictions, while the y-error bars are the binomial based 95% confidence intervals in the real underlying frequency for each structural class. The red circle surrounds the point corresponding to all compounds that do not belong to any of the structural classes. The labels correspond to structural classes as illustrated in Figure 2.

The compounds with excess potent binders correspond to a range of -8.7 to -5.0 in terms of quantum mechanically computed binding energy to Fe^{III} in its doublet state, and the other groups binding energies are in the range -6.2 to $+1.3$ kcal/mol. The corresponding energy ranges are $+0.2$ to $+2.8$ kcal/mol for the enhanced binders to Fe^{III} sextet compared to $+1.2$ to $+4.3$ kcal/mol for nonenhanced binders and -6.5 to -3.1 kcal/mol for enhanced binders to Fe^{II} singlet compared to -8.1 to $+3.8$ kcal/mol for nonenhanced binders. This is illustrated in Figure 7; binding to the doublet state of Fe^{III} might best discriminate between compounds that show an enhanced inhibition and those that do not. Structural classes with a computed binding energy to Fe^{III} doublet state that is below about -4.5 kcal/mol show a clear tendency to be among

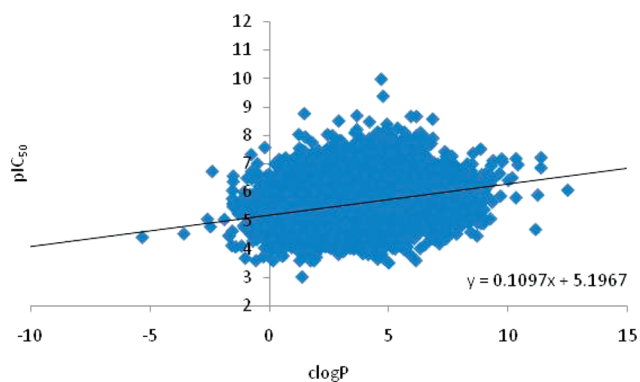


Figure 6. Maximum pIC₅₀ achieved by a given compound plotted against the clogP of that compound. In this plot the compounds where the maximum pIC₅₀ remains outside the dynamic range of the assay have been excluded.

the most potent compounds, and the lower that value is beyond -4.5 kcal/mol, the more likely the structural class is to be potent. Apart from the one point in the center of the plot (the isoquinoline structural class), compounds with a binding energy below $+2.5$ kcal/mol to the sextet state show a similar trend. 2-Methylpyridine is a remarkably poor binder to Fe^{III} doublet state having a value of $+1.3$ kcal/mol. This might explain why this substructure is particularly beneficial in preventing CYP inhibition (Figure 5). Binding to Fe^{II} in a singlet state does not show any clear correlation with inhibition.

A countervailing ability of these heteroaromatic nitrogen atoms is to form hydrogen bonds, particularly with water in solution (Scheme 3). Such solvation effects (or even protonation in extremis) could be responsible for the deviation away from the line seen by the 2-methylpyridine structure class in Figure 5. In order to very crudely estimate the ability of each heterocycle to form hydrogen bonds with water, the complex of each with a single molecule of water has been optimized but with the oxygen atom of water constrained to be along the lone pair axis of the nitrogen atom (structures and energies are in Supporting Information). As with the complexation energies with iron, these are gas-phase calculations and represent these solvent effects in a very crude way that emphasizes the role of the heteroaromatic nitrogen atoms. Two types of related experimental characterizations have been obtained also. These are taken from the work of Laurence et al. and describe hydrogen-bonding strength with pK_{BHX} and protonation ability as pK_{BH+}.⁶¹ These energies are given in Table 4 and are plotted against the binding energy for Fe^{III} doublet in Figure 8 alongside a modified version of Figure 7 in which the calculated binding energy to water is subtracted from the binding energy to the doublet state of Fe^{III}. The equivalent plots for the other states are shown in the Supporting Information. This shows that the 2-methylpyridine (6) and quinoline (7) are able to form strong interactions with water despite the diminished interaction computed with iron. This reflects the smaller size of water molecules contrasting with the constricted environment of heme-bound iron. The electron donation effect of the 2-methyl group enhances the hydrogen-bond acceptor ability of the adjacent pyridine nitrogen, but its steric protrusion prevents this translating into binding to iron.

It is notable that neither hydrogen-bond acceptor ability as computed or measured nor basicity (Table 4) are able to rationalize

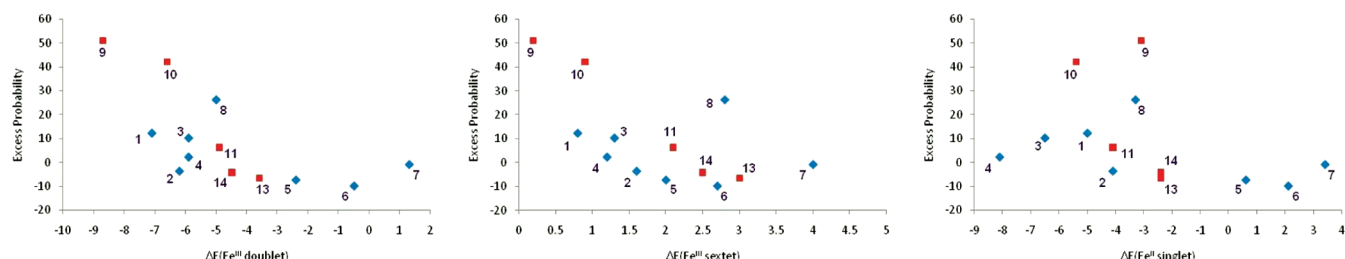
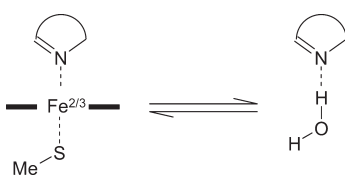


Figure 7. Excess probability for each structural class taken from Table 3 is plotted against the binding energy to the three different spin states of iron taken from Table 1. Points in blue are six-membered ring heterocycles, and those in red are five-membered rings. The left-hand panel is for binding to Fe^{III} doublet state, the center for the sextet state, and the right-hand for binding to Fe^{II} singlet state. The numbers next to each point correspond to the structural classes illustrated in Figure 2.

Scheme 3. Interaction with Iron Is Balanced against Hydrogen Bonding in Solution to Determine the Observed Binding Ability of Each Structural Class



the observed enhanced inhibition of CYPs. In particular, quinoline and 2-methylpyridine are very strong acceptors and yet do not show enhanced inhibition; on the contrary, these two structural classes tend to show diminished inhibition. These are clearly varied by steric effects. Less straightforward to explain is that oxazole which shows substantially enhanced inhibition is a very poor hydrogen-bond acceptor and a weak base. The weak hydrogen-bond acceptor ability of oxazole does contribute toward the enhanced inhibition in the sense that, whereas imidazole has the strongest computed interaction with iron, it also has the strongest interaction with water which tends to favor remaining in aqueous solution rather than binding. Whereas oxazole, which has the third highest computed interaction energy with Fe^{III} doublet state, has the seventh highest computed and eighth highest measured interaction energy as a hydrogen-bond acceptor so provides a much weaker solvation energy. It therefore favors the equilibrium in Scheme 3 being shifted to the left. These two effects overall contribute to oxazole having an enhanced inhibition, almost the same as imidazole and higher than pyridine which is computed to have a higher binding energy to both iron and water.

The correspondence between the computed complexation energies with iron and experimentally observed inhibition suggests that such calculations can be a useful way of interpreting such data. The 2-fluoro and 2-methyl examples suggest that it can be a useful approach to interpreting SAR, particularly the complex interplay between electronic and steric effects in these binding events. As with many techniques that allow expectations to be set of a given compound, outliers can be identified, and these can provide insight into how to defy expectation.^{62,63} For instance, among the imidazole structural class, there are seven compounds with the substructure shown in Figure 9, none of which are in the top 10% of all compounds. For this set of compounds, the maximum pIC_{50} is 6.1, and two of the compounds have maximum pIC_{50} values < 5. These compounds suggest follow up calculations to investigate whether this might

Table 4. Interaction Energy between Heteroaromatic Nitrogen Atoms and a Water Molecule Computed As Described in the Text and the Hydrogen-Bond Strength (pK_{BHX}) and Basicity ($\text{pK}_{\text{BH}+}$) Taken from the Work of Laurence et al⁶¹

ligand	water interaction		$\text{pK}_{\text{BH}+}$
	energy (kcal/mol)	pK_{BHX}	
1 pyridine	-7.3	1.86	5.20
2 pyridazine	-7.3	1.65	2.00
3 pyrimidine	-6.3	1.07	0.93
4 pyrazine	-6.1	0.92	0.37
5 2-fluoropyridine	-6.3	0.95	-0.44
6 2-methylpyridine	-9.0	2.03	5.96
7 quinoline	-8.5	1.89	4.85
8 isoquinoline	-7.4	1.94	5.40
9 N-methylimidazole	-8.3	2.72	7.12
10 oxazole	-6.5	1.30	0.80
11 thiazole	-5.7	1.37	2.52
12 isoxazole	-5.9	0.81	1.30
13 isothiazole	-5.8	—	—
14a 1-methyltetrazole (3 linked to Fe)	-4.2	—	—
14b 1-methyltetrazole (4 linked to Fe)	-6.7	—	—

be due to moderation of the interaction with iron or to other effects.

Analogous plots to Figure 5 have been created for each of the five main isoforms that are studied and are shown in Figure 10, while the summary data for each isoform are given in Supporting Information. Plots analogous to Figures 4 and 6 illustrating the lipophilicity dependence of each set of data have also been generated and are also in the Supporting Information. The plots in Figure 10 show that there are certain variations between the isoforms in terms of their propensity to show enhanced inhibition for this set of potential iron binding ligands. Notably, the variation away from the 1:1 line is smaller for 1A2 and 2D6, and both have two structural classes that are away from the line in a downward direction. The other three isoforms show a similar spread of points as in Figure 5. Of the structural classes, three show significantly enhanced inhibition in all isoforms: imidazole, oxazole, and pyridine. The 2-methylpyridine structural class shows a significant deviation in the other direction for all isoforms. The other structural classes that show enhanced binding in only some isoforms are: pyrimidine (1A2, 2C9, 2D6, and 3A4), pyrazine (1A2,

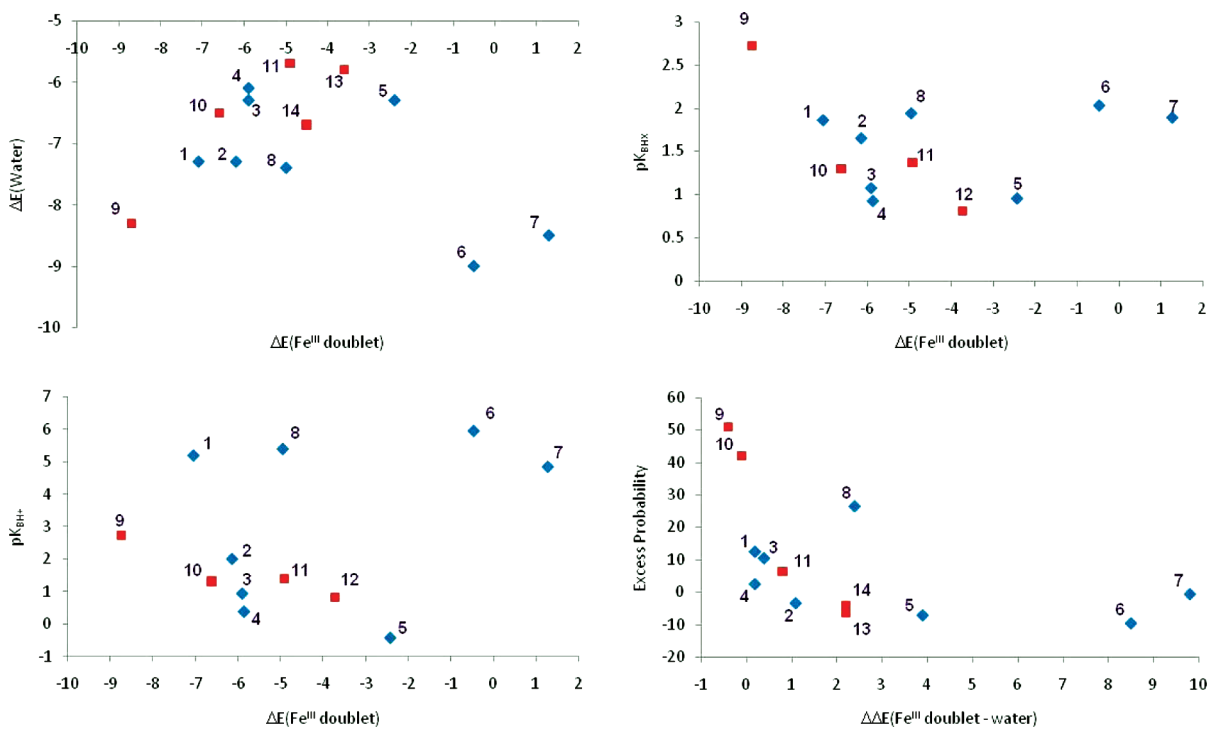


Figure 8. In the top left-hand panel, complexation energies to Fe^{III} doublet state are compared to those computed for interaction with water, and the difference between the two is plotted in the bottom right-hand panel with the corresponding excess probability on the vertical axis. In the top right panel are shown the computed interaction energies with Fe^{III} doublet state plotted against measured hydrogen-bond acceptor strength and in bottom left against basicity, both as reported by Laurence et al.⁶¹ Points in blue are six-membered rings, and those in red are five-membered rings. Numbering is according to structural classes indicated in Figure 2.

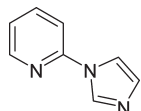


Figure 9. A substructural type found within the imidazole class that is not associated with the same enhanced likelihood of being a potent compound as the structural class more generally.

2C19, 2D6, and 3A4), quinoline (2C9), isoquinoline (2C19, 2D6, and 3A4), and thiazole (2C9, 2C19, and 3A4). Structural classes that show significantly reduced binding in only some isoforms are pyridazine (1A2), quinoline (2D6), and tetrazole (2D6). The quinoline structural class has remarkably varying behavior, and this might correspond to the unusual steric environment in which the quinoline nitrogen is situated. All of the isoform data suggest that the steric environment of the heme is a critical feature that determines the behavior of the structural classes across the isoforms. Some structural classes are sufficiently good ligands for iron that they show enhanced inhibition regardless. The three structures computed to have the best binding energies to Fe^{III} in its doublet state (all better than -6.6 kcal/mol) are the three classes that show cross-isoform activity. This further supports that this is the relevant state of iron for our inhibition assays. Other structural classes show more subtle isoform dependent enhancements reflecting a weaker interaction with iron that entails a greater susceptibility to steric effects preventing binding to the iron atom.

The final set of data that has been studied derives from protein crystal structures of the various isoforms of the P450s. To

investigate whether the steric environment of the iron atom corresponds with the observations discussed in the previous paragraph, the crystal structures of the four relevant isoforms that are available have been examined. For 1A2, there is only one crystal structure available with pdb code 2HI4.²² For 2C9 there are three structures available: 2R9O, 1OG2, and 1OG5.^{23,64} For 2D6 there is only one structure available, 2F9Q.²⁴ For 3A4 there are four available structures, 3NXU, 2V0M, 2J0D, and 1TQN.^{25,26,65} Although quantitative deductions are challenging, the iron is in a very exposed environment in 3A4 and a crowded environment in 2D6 with the other two isoforms intermediate between these two extremes. The flexibility of these binding sites would need to be well understood before more definitive deductions could be made, but such calculations will require improved parametrization of the iron atom which the calculations described here ought to contribute toward.

Across all isoforms and all species, there are a number of structures of cytochrome P450s with ligands of the type being studied here included. These were identified with a keyword search of the PDB for "P450" and a subsequent manual inspection of the ligands involved. Only two of the structural classes are represented: imidazoles and pyridines. These have been surveyed for some geometrical parameters that can be related to those obtained in the quantum mechanical calculations. In particular, the distance between Fe and the binding nitrogen atom and the distance between Fe and the cysteine's sulfur atom. The angle formed at iron by the N–Fe–S linkage has also been measured for each structure along with three dihedrals all illustrated in Figure 11. The values in the set of structures are shown as distributions, and the category into which the QM optimized

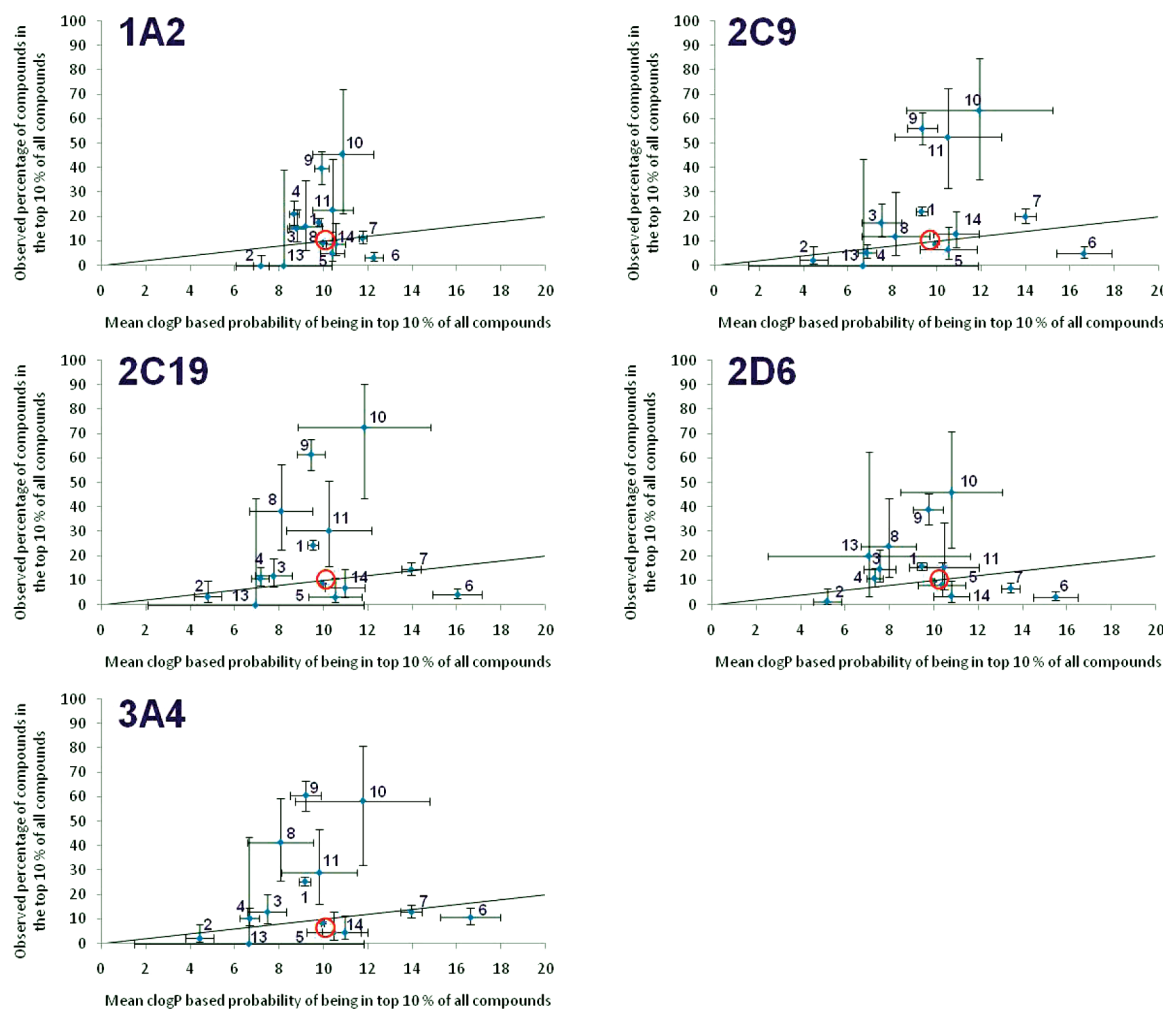


Figure 10. Plots equivalent to that shown in Figure 5 but for inhibition of each of the five major isoforms studied.

equivalents for imidazole and pyridine in the three states of iron are indicated with arrows. Full lists of individual values are given in the Supporting Information. Most crystallographic experiments intend to study the heme in its resting state with Fe^{III} bound. However, the X-ray experiment itself can perform reductions, and so it is possible that the observed structures might have the iron reduced to Fe^{II} or that there could be a mix of the two oxidation states present in the experiment.^{66,67} Over the six geometric parameters examined, the best agreement is with the quantum mechanical geometries obtained for Fe^{III} in its doublet state. A survey of computed geometric parameters for a number of complexes with varying axial ligands had suggested that B3LYP might perform worse than other functionals, although the errors were suggested to be less than 0.1 Å, consistent with the results obtained here.⁶⁸ As in much of the computational work, the focus for Rydberg et al had been on a range of complexes with small ligands and in varying spin and oxidation states that might be relevant to the catalytic mechanism.

One geometric parameter that was examined has values in all crystal structures that are within a few degrees of one another and which none of the computed geometries reproduce. This is the dihedral angle at which the carbon sulfur bond of the cysteine (or SMe) is oriented relative to the porphyrin ligand. In order

to investigate whether this has a marked effect on computed geometries or energies, the complexes for Fe^{III} in its doublet state were reoptimized but with the C–S–Fe–N dihedral constrained to 10.7°, which is the mean value observed in all 84 complexes examined. The resulting energies of complexation and perturbed Fe–N and Fe–S distances are given in Table 5. The constrained energies correlate very tightly with those that are unconstrained and show an offset of ~0.2 kcal/mol. The Fe–S distance remains little changed, and for the most part the Fe–N distance also changes little, but isoxazole and isothiazole both form complexes with slightly longer bonds (by 0.02 and 0.03 Å). The N-methylimidazole and pyridine complexes in the constrained orientation have values of the geometric parameters illustrated in Figure 11 that are better in line with those observed. This constraint of the orientation of the S–C bond imposed by the protein does not seem to have a profound effect upon the binding energies or geometries according to the quantum mechanical calculations, and this is consistent with the high degree of geometric flexibility predicted by the contour plots shown in Figure 1. The high correlation suggests that future studies could employ either the fully optimized or the constrained geometries fairly interchangeably.

Finally, having studied a set of known structures, a set of so-called “heteroaromatic rings of the future” predicted by Pitt et al.

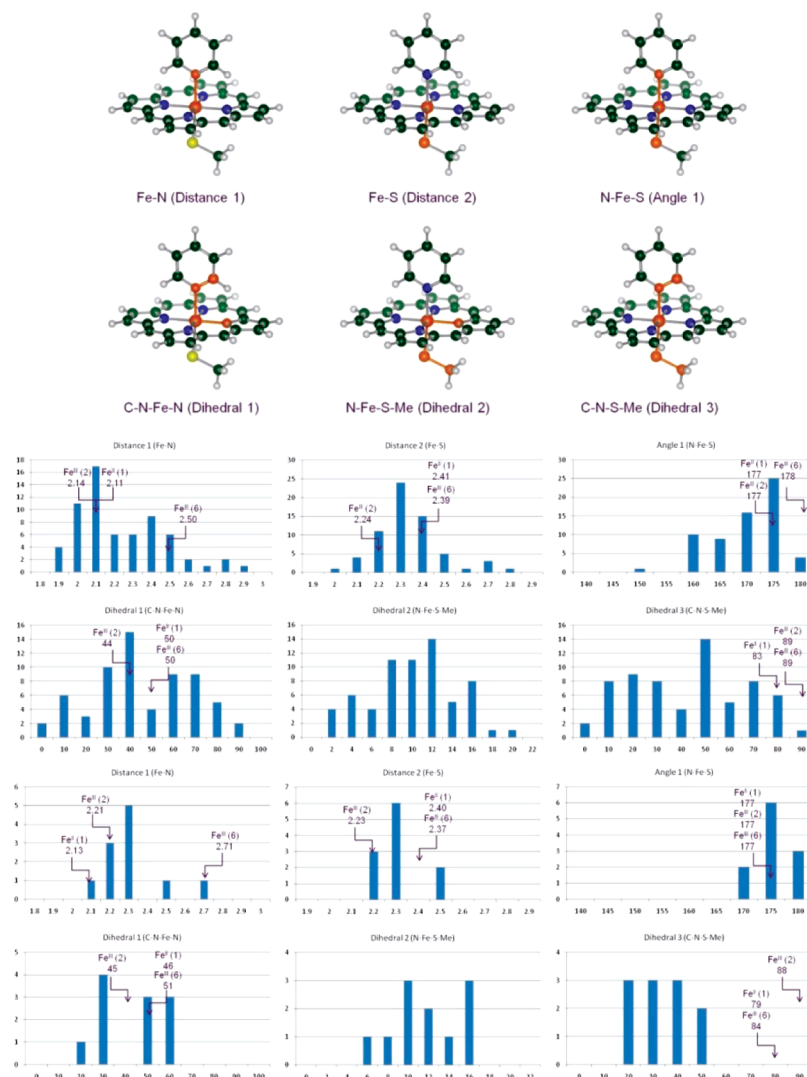


Figure 11. Values of key geometric parameters observed in the relevant crystal structures of heteroaromatic ligands binding to cytochromes P450. The molecular visualizations at the top illustrate the two distances, one angle, and three dihedrals, whose values are plotted for complexes with imidazoles in the middle and pyridines at the bottom. Values obtained in the quantum mechanical optimizations for the various oxidation and spin states are indicated by arrows.

to be synthesizable have been studied.⁴³ A great strength of quantum mechanical methods is that they do not rely upon parametrization which would limit their domain of application; they should apply equally well to these as yet unknown structures as they do to those that are well exemplified. With this in mind, the set of heteroaromatic ring systems highlighted by Pitt et al. and illustrated in Figure 12 has been computed in complex with Fe^{III} in its doublet and sextet states. In some cases the rings are capable of populating more than one tautomer, but for the sake of simplicity, only those tautomers originally presented have been studied. Some examples incorporate more than one potential chelating nitrogen, and in these cases, both have been examined.

The data presented in Table 6 suggest that most of the heterocycles proposed do not pose an elevated risk of inhibiting P450s which would require ΔE to the doublet state below about -4.5 kcal/mol (Figure 7). They can nevertheless be placed in order of risk according to this binding energy. The five most likely ring heteroatomic nitrogen types to shown

enhanced P450 inhibition are **25**, **17**, **21**, **18**, and **22b**. This suggests that nitrogens in a five-membered ring are more likely to inhibit than those in six-membered rings, particularly if there is an adjacent donor. Contrasting with **19** and **26** suggests that an extra acceptor protruding toward the binding nitrogen can decrease the risk of binding. These two observations suggest that groups in the proximity of the binding nitrogen atom are influential. It also suggests that bidentate ligands, which **19** and **26** could be, are not beneficial in this particular environment.

EXPERIMENTAL AND COMPUTATIONAL PROCEDURES

Inhibitors of recombinant versions of the five dominant human isoforms of the cytochromes P450 were assessed for their ability to inhibit the turnover of a number of standard (fluorescent) substrates. The data for inhibition of different

substrates have been merged. The substrates for each isoform are as follows:

- 1A2: Phenacetin, 3-cyano-7-ethoxycoumarin, ethoxyresorufin, and methoxyresorufin.
- 2C9: Tolbutamide, naproxen, diclofenac, and 7-methoxy-4-trifluoromethyl-coumarin.
- 2C19: Diazepam, S-mephentoin, 7-methoxy-4-(trifluoromethyl)-coumarin, and 3-cyano-7-ethoxycoumarin.
- 2D6: Dextromethorphan, 3-[2-(*N,N*-diethyl-*N*-methyl-ammonium)ethyl]-7-methoxy-4-methylcoumarin, 7-methoxy(aminomethyl)-coumarin, and bufurrol.
- 3A4: Erythromycin, 7-benzoyloxy-4-trifluoromethylcoumarin, and midazolam.

In all cases pIC_{50} values are analyzed.

All quantum mechanical calculations were performed in Gaussian03 or Gaussian09.^{50,51} The B3LYP functional was

Table 5. Perturbed Complexation Energies and Fe–N and Fe–S Distances Observed in B3LYP Optimized Complexes of Heteroaromatic Compounds^a

ligand	ΔE to Fe^{III} doublet heme (kcal/mol)	Fe–N (Å)	Fe–S (Å)
1 pyridine	−6.9	2.21	2.23
2 pyridazine	−6.0	2.19	2.23
3 pyrimidine	−5.8	2.22	2.22
4 pyrazine	−5.7	2.22	2.22
5 2-fluoropyridine	−2.2	2.42	2.23
6 2-methylpyridine	−0.1	2.67	2.23
7 quinoline	1.7	2.68	2.23
8 isoquinoline	−4.9	2.21	2.23
9 <i>N</i> -methylimidazole	−8.9	2.13	2.23
10 oxazole	−6.7	2.16	2.22
11 thiazole	−5.0	2.20	2.22
12 isoxazole	−3.9	2.18	2.21
13 isothiazole	−3.7	2.19	2.22
14a 1-methyltetrazole (3 linked to Fe)	−1.7	2.21	2.22
14b 1-methyltetrazole (4 linked to Fe)	−4.6	2.17	2.22

^aWhen the alkyl group on sulfur is constrained to a position more closely mimicking that observed in crystal structures than in the fully optimized complex.

employed combined with the 6-31G* basis set and the lanl2dz basis set and core pseudopotential for iron.^{44–49} All full optimizations were characterized by frequency calculations which occasionally reported low negative values, but dihedral scans revealed these to be artifacts of the frequency calculation

Table 6. Complexation Energies Computed in a Similar Fashion to Those in Table 1 for a Set of “Heteroaromatic Rings of the Future” Proposed by Pitt et al.⁴³ ^a

nitrogen atom bound to iron	ΔE Fe^{III} doublet state	ΔE Fe^{III} sextet state
15a	−2.6	3.9
15b	1.0	4.0*
16a	−1.9	3.9
16b	−1.9	4.4
17	−4.1*	3.6
18	−3.4*	1.5*
19	3.8	5.7*
20	0.5*	5.7
21	−4.0*	2.6*
22a	0.3	5.1*
22b	−3.4	4.4
23a	2.2	4.3
23b	−2.1	4.1
24	−2.5	4.6*
25	−7.3*	0.7
26	−1.7	3.6
27	−3.4	3.5
28	−3.3	4.0
29	−3.0	3.8
30a	2.2	5.0
30b	1.5	—
31a	−3.1	4.5
31b	1.1	—
32a	−2.5	31.6
32b	3.1	—

^a Binding to Fe^{III} in its doublet and sextet state has been computed. Entries marked with — did not retain the Fe–N bond, and the ligand drifted away to form alternative interactions which are unlikely to be of biochemical relevance. Entries marked with * have a negative frequency corresponding to rotation about the Fe–N bond.

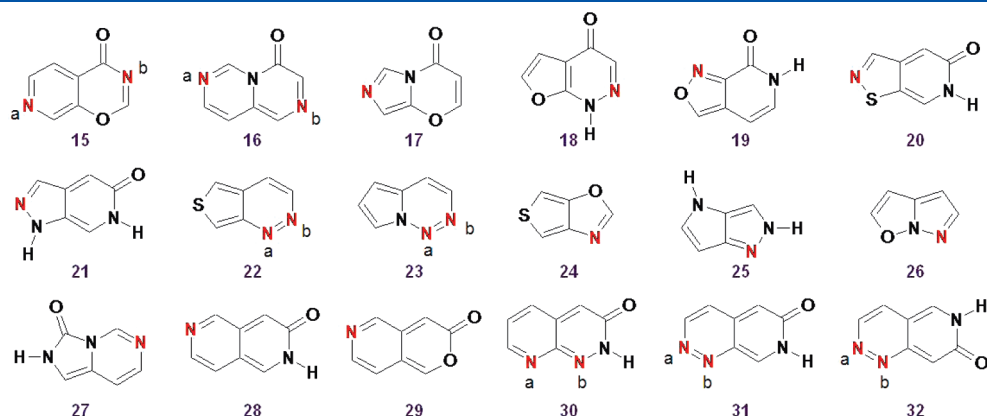


Figure 12. Heteroaromatic rings proposed by Pitt et al.⁴³ that have been studied with quantum mechanics.

method. Scans of the dihedrals about the Fe–S and Fe–N bonds employed the opt=(modredundant,loose) keyword.

CONCLUSIONS

Quantum mechanical calculations can optimize complexes of heme-bound iron with SMe and heteroaromatic nitrogen ligands in the fifth and sixth sites of an octahedron. The heteroaromatic ring and the S-Me are computed to have very low barriers to rotation about the N–Fe–S axis. The geometries of these complexes in which iron is Fe^{III} and in a doublet spin state are in good agreement with crystallographic structures of such ligands bound to cytochrome P450 enzymes. In the crystal structures the alkyl group on sulfur is constrained to one particular orientation, and quantum mechanical calculations suggest only a small energy penalty to achieve this orientation and with little effect on the binding of the heteroaromatic ligands either in terms of energy or geometry by the perturbed orientation of the SMe. The energies of complexation computed for these ligands rank as tightest binding those heteroaromatic rings that are observed to be most potent inhibitors in experimental assays of cytochrome P450 inhibition, especially when weighted for lipophilicity-based expectation. Tighter binding ligands are predicted to increase the doublet–sextet gap for Fe^{III}, and this might be experimentally detectable. The analysis of inhibition of cytochrome P450 can be done in such a way that lipophilicity is factored out and enhanced inhibition caused by specific interactions, covalent bonds to iron in this case, can be detected. The related trend for interaction between the heteroaromatic nitrogen atoms and water can be used to explain how some ring types decrease the risk of interacting with iron. These computed values alongside experimental measurements demonstrate that interaction with the iron in CYPs is significantly different from hydrogen-bond acceptor ability. Ring types that maintain hydrogen-bonding ability while decreasing iron binding are of high medicinal chemistry interest as they ought to bring the benefits of decreased lipophilicity without increased molecular weight or risk of inhibiting cytochrome P450s compared to the ring in which the nitrogen atom is replaced with carbon. Binding to the different isoforms of P450 is sensitive to potential iron binding groups to different extents: 3A4, 2C9, and 2C19 are most sensitive to iron binding, and 1A2 and 2D6 are less sensitive. Calculations on binding of as yet unknown ring types can be performed, and the set studied here suggests that bidentate ligands do not bind more tightly to this particular metal environment. Modeling the binding event as closely as possible is generally to be preferred and is shown here to provide a coherent view of observed inhibition and geometries. The values contrast with hydrogen-bond formation and protonation strengths principally because of the close proximity of the heme ligand once the bond to iron is formed; this ligand provides a very particular steric and electronic environment.

ASSOCIATED CONTENT

Supporting Information. All quantum mechanical geometries and energies, binding energies including vibrational corrections, SMARTS definitions for structural classes, data summaries and lipophilicity dependence of inhibition of individual isoforms, binding energies to iron minus binding to water compared to excess probability, and geometry parameters obtained from PDB files. This information is available free of charge via the Internet at <http://pubs.acs.org/>.

AUTHOR INFORMATION

Corresponding Author

*E-mail: andrew.leach@astrazeneca.com.

REFERENCES

- (1) Lipinski, C. A.; Lombardo, F.; Dominy, B. W.; Feeney, P. J. Experimental and computational approaches to estimate solubility and permeability in drug discovery and development settings. *Adv. Drug Delivery Rev.* **1997**, *23*, 3–25.
- (2) Leeson, P. D.; Springthorpe, B. The influence of drug-like concepts on decision-making in medicinal chemistry. *Nat. Rev. Drug Discovery* **2007**, *6*, 881–890.
- (3) Hughes, J. D.; Blagg, J.; Price, D. A.; Bailey, S.; DeCrescenzo, G. A.; Devraj, R. V.; Ellsworth, E.; Fobian, Y. M.; Gibbs, M. E.; Gilles, R. W.; Greene, N.; Huang, E.; Krieger-Burke, T.; Loesel, J.; Wager, T.; Whiteley, L.; Zhang, Y. Physicochemical drug properties associated with in vivo toxicological outcomes. *Bioorg. Med. Chem. Lett.* **2008**, *18*, 4872–4875.
- (4) Waring, M. J. Defining optimum lipophilicity and molecular weight ranges for drug candidates—Molecular weight dependent lower log D limits based on permeability. *Bioorg. Med. Chem. Lett.* **2009**, *19*, 2844–2851.
- (5) Guengerich, F. P. Common and Uncommon Cytochrome P450 Reactions Related to Metabolism and Chemical Toxicity. *Chem. Res. Toxicol.* **2001**, *14*, 611–650.
- (6) Lamb, D. C.; Waterman, M. R.; Kelly, S. L.; Guengerich, F. P. Cytochromes P450 and drug discovery. *Curr. Opin. Biotechnol.* **2007**, *18*, 504–512.
- (7) Guengerich, F. P. Cytochrome P450 and Chemical Toxicology. *Chem. Res. Toxicol.* **2008**, *21*, 70–83.
- (8) Kola, I.; Landis, J. Opinion: Can the pharmaceutical industry reduce attrition rates? *Nat. Rev. Drug Discovery* **2004**, *3*, 711–716.
- (9) Obach, R. S. Inhibition of drug-metabolizing enzymes and drug-drug interactions in drug discovery and development. In *Drug-Drug Interactions in Pharmaceutical Development*; Li, A. P., Ed.; John Wiley and Sons: Hoboken, NJ, 2008; pp 75–93.
- (10) Bibi, Z. Role of cytochrome P450 in drug interactions. *Nutr. Metab.* **2008**, *5*, 27.
- (11) *Drug-Drug Interactions in Pharmaceutical Development*; Li, A. P., Ed.; John Wiley and Sons: Hoboken, NJ, 2008.
- (12) Lewis, D. F. V. Human cytochromes P450 associated with the phase 1 metabolism of drugs and other xenobiotics: A compilation of substrates and inhibitors of the CYP1, CYP2 and CYP3 families. *Curr. Med. Chem.* **2003**, *10*, 1955–1972.
- (13) Guengerich, F. P. Oxidative, reductive, and hydrolytic metabolism of drugs. In *Drug Metabolism in Drug Design and Development*; Zhang, D., Zhu, M., Humphreys, W. G., Eds.; John Wiley and Sons: Hoboken, NJ, 2008; pp 15–35.
- (14) Obach, R. S.; Walsky, R. L.; Venkatakrishnan, K.; Houston, J. B.; Tremaine, L. M. In vitro cytochrome P450 inhibition data and the prediction of drug-drug interactions: Qualitative relationships, quantitative predictions, and the rank-order approach. *Clin. Pharmacol. Ther.* **2005**, *78*, 582–592.
- (15) Shaik, S.; Kumar, D.; de Visser, S. P.; Altun, A.; Thiel, W. Theoretical perspective on the structure and mechanism of cytochrome P 450 enzymes. *Chem. Rev.* **2005**, *105*, 2279–2328.
- (16) Shaik, S.; Lai, W.; Chen, H.; Wang, Y. The Valence Bond Way: Reactivity Patterns of Cytochrome P450 Enzymes and Synthetic Analogs. *Acc. Chem. Res.* **2010**, *43*, 1154–1165.
- (17) Li, C.; Zhang, L.; Zhang, C.; Hirao, H.; Wu, W.; Shaik, S. Which oxidant is really responsible for sulfur oxidation by cytochrome P450? *Angew. Chem., Int. Ed.* **2007**, *46*, 8168–8170.
- (18) *The Porphyrins, Vol. III: Physical Chemistry Part A*; Dolphin, D., Ed.; Academic Press Inc.: New York, 1978.
- (19) Jefcoate, C. R. Measurement of substrate and inhibitor binding to microsomal cytochrome P-450 by optical-difference spectroscopy. *Methods Enzymol.* **1978**, *52*, 258–279.

- (20) Poulos, T. L.; Finzel, B. C.; Gunsalus, I. C.; Wagner, G. C.; Kraut, J. The 2.6-ANG. crystal structure of *Pseudomonas putida* cytochrome P-450. *J. Biol. Chem.* **1985**, *260*, 16122–16130.
- (21) Poulos, T. L.; Finzel, B. C.; Howard, A. J. High-resolution crystal structure of cytochrome P450cam. *J. Mol. Biol.* **1987**, *195*, 687–700.
- (22) Sansen, S.; Yano, J. K.; Reynald, R. L.; Schoch, G. A.; Griffin, K. J.; Stout, C. D.; Johnson, E. F. Adaptations for the Oxidation of Polycyclic Aromatic Hydrocarbons Exhibited by the Structure of Human P450 1A2. *J. Biol. Chem.* **2007**, *282*, 14348–14355.
- (23) Williams, P. A.; Cosme, J.; Ward, A.; Angove, H. C.; Matak, V. D.; Jhoti, H. Crystal structure of human cytochrome P450 2C9 with bound warfarin. *Nature* **2003**, *424*, 464–468.
- (24) Rowland, P.; Blaney, F. E.; Smyth, M. G.; Jones, J. J.; Leydon, V. R.; Oxbridge, A. K.; Lewis, C. J.; Tennant, M. G.; Modi, S.; Eggleston, D. S.; Chenery, R. J.; Bridges, A. M. Crystal structure of human cytochrome P 450 2D6. *J. Biol. Chem.* **2006**, *281*, 7614–7622.
- (25) Yano, J. K.; Wester, M. R.; Schoch, G. A.; Griffin, K. J.; Stout, C. D.; Johnson, E. F. The Structure of Human Microsomal Cytochrome P450 3A4 Determined by X-ray Crystallography to 2.05-ANG. Resolution. *J. Biol. Chem.* **2004**, *279*, 38091–38094.
- (26) Ekroos, M.; Sjögren, T. Structural basis for ligand promiscuity in cytochrome P 450 3A4. *Proc. Natl. Acad. Sci. U.S.A.* **2006**, *103*, 13682–13687.
- (27) Afzelius, L.; Zamora, I.; Masimirembwa, C. M.; Karlen, A.; Andersson, T. B.; Muccetti, S.; Baroni, M.; Cruciani, G. Conformer- and Alignment-Independent Model for Predicting Structurally Diverse Competitive CYP2C9 Inhibitors. *J. Med. Chem.* **2004**, *47*, 907–914.
- (28) De Groot, M. J.; Ackland, M. J.; Horne, V. A.; Alex, A. A.; Jones, B. C. Novel Approach To Predicting P450-Mediated Drug Metabolism: Development of a Combined Protein and Pharmacophore Model for CYP2D6. *J. Med. Chem.* **1999**, *42*, 1515–1524.
- (29) De Groot, M. J.; Alex, A. A.; Jones, B. C. Development of a Combined Protein and Pharmacophore Model for Cytochrome P450 2C9. *J. Med. Chem.* **2002**, *45*, 1983–1993.
- (30) Kemp, C. A.; Flanagan, J. U.; van Eldik, A. J.; Marechal, J.; Wolf, C. R.; Roberts, G. C. K.; Paine, M. J. I.; Sutcliffe, M. J. Validation of Model of Cytochrome P450 2D6: An in Silico Tool for Predicting Metabolism and Inhibition. *J. Med. Chem.* **2004**, *47*, 5340–5346.
- (31) Kemp, C. A.; Marechal, J.; Sutcliffe, M. J. Progress in cytochrome P 450 active site modeling. *Arch. Biochem. Biophys.* **2005**, *433*, 361–368.
- (32) Kirton, S. B.; Kemp, C. A.; Tomkinson, N. P.; St-Gallay, S.; Sutcliffe, M. J. Impact of incorporating the 2C5 crystal structure into comparative models of cytochrome P450 2D6. *Proteins: Struct., Funct., Genet.* **2002**, *49*, 216–231.
- (33) Kjellander, B.; Masimirembwa, C. M.; Zamora, I. Exploration of Enzyme-Ligand Interactions in CYP2D6 & 3A4 Homology Models and Crystal Structures Using a Novel Computational Approach. *J. Chem. Inf. Model.* **2007**, *47*, 1234–1247.
- (34) Lill, M. A.; Dobler, M.; Vedani, A. Prediction of small-molecule binding to cytochrome P450 3A4: flexible docking combined with multidimensional QSAR. *ChemMedChem* **2006**, *1*, 73–81.
- (35) Lewis, D. F. V.; Jacobs, M. N.; Dickins, M. Compound lipophilicity for substrate binding to human P450s in drug metabolism. *Drug Discovery Today* **2004**, *9*, 530–537.
- (36) Gleeson, M. P. Generation of a set of simple, interpretable ADMET rules of thumb. *J. Med. Chem.* **2008**, *51*, 817–834.
- (37) Waring, M. J. Lipophilicity in drug discovery. *Expert Opin. Drug Discovery* **2010**, *5*, 235–248.
- (38) Refsgaard, H. H. F.; Jensen, B. F.; Christensen, I. T.; Hagen, N.; Brockhoff, P. B. In silico prediction of cytochrome P450 inhibitors. *Drug Dev. Res.* **2006**, *67*, 417–429.
- (39) Shaik, S.; Cohen, S.; Wang, Y.; Chen, H.; Kumar, D.; Thiel, W. P 450 Enzymes: Their structure, reactivity, and selectivity - modeled by QM/MM calculations. *Chem. Rev.* **2010**, *110*, 949–1017.
- (40) Shaik, S.; Kumar, D.; de Visser, S. P. A Valence Bond Modeling of Trends in Hydrogen Abstraction Barriers and Transition States of Hydroxylation Reactions Catalyzed by Cytochrome P450 Enzymes. *J. Am. Chem. Soc.* **2008**, *130*, 10128–10140.
- (41) Meunier, B.; de Visser, S. P.; Shaik, S. Mechanism of Oxidation Reactions Catalyzed by Cytochrome P450 Enzymes. *Chem. Rev.* **2004**, *104*, 3947–3980.
- (42) Balding, P. R.; Porro, C. S.; McLean, K. J.; Sutcliffe, M. J.; Marechal, J.; Munro, A. W.; de Visser, S. P. How Do Azoles Inhibit Cytochrome P450 Enzymes? A Density Functional Study. *J. Phys. Chem. A* **2008**, *112*, 12911–12918.
- (43) Pitt, W. R.; Parry, D. M.; Perry, B. G.; Groom, C. R. Heteroaromatic Rings of the Future. *J. Med. Chem.* **2009**, *52*, 2952–2963.
- (44) Becke, A. D. Density-functional thermochemistry. III. The role of exact exchange. *J. Chem. Phys.* **1993**, *98*, 5648–5652.
- (45) Lee, C.; Yang, W.; Parr, R. G. Development of the Colle-Salvetti correlation-energy formula into a functional of the electron density. *Phys. Rev. B: Condens. Matter* **1988**, *37*, 785–789.
- (46) Hariharan, P. C.; Pople, J. A. Influence of polarization functions on MO hydrogenation energies. *Theor. Chim. Acta* **1973**, *28*, 213–222.
- (47) Hay, P. J.; Wadt, W. R. Ab initio effective core potentials for molecular calculations. Potentials for the transition metal atoms scandium to mercury. *J. Chem. Phys.* **1985**, *82*, 270–283.
- (48) Hay, P. J.; Wadt, W. R. Ab initio effective core potentials for molecular calculations. Potentials for potassium to gold including the outermost core orbitals. *J. Chem. Phys.* **1985**, *82*, 299–310.
- (49) Wadt, W. R.; Hay, P. J. Ab initio effective core potentials for molecular calculations. Potentials for main group elements sodium to bismuth. *J. Chem. Phys.* **1985**, *82*, 284–298.
- (50) Frisch, M. J.; Trucks, G. W.; Schlegel, H. B.; Scuseria, G. E.; Robb, M. A.; Cheeseman, J. R.; Montgomery, J. A., Jr.; Vreven, T.; Kudin, K. N.; Burant, J. C.; Millam, J. M.; Iyengar, S. S.; Tomasi, J.; Barone, V.; Mennucci, B.; Cossi, M.; Scalmani, G.; Rega, N.; Petersson, G. A.; Nakatsuji, H.; Hada, M.; Ehara, M.; Toyota, K.; Fukuda, R.; Hasegawa, J.; Ishida, M.; Nakajima, T.; Honda, Y.; Kitao, O.; Nakai, H.; Klene, M.; Li, X.; Knox, J. E.; Hratchian, H. P.; Cross, J. B.; Bakken, V.; Adamo, C.; Jaramillo, J.; Gomperts, R.; Stratmann, R. E.; Yazyev, O.; Austin, A. J.; Cammi, R.; Pomelli, C.; Ochterski, J. W.; Ayala, P. Y.; Morokuma, K.; Voth, G. A.; Salvador, P.; Dannenberg, J. J.; Zakrzewski, V. G.; Dapprich, S.; Daniels, A. D.; Strain, M. C.; Farkas, O.; Malick, D. K.; Rabuck, A. D.; Raghavachari, K.; Foresman, J. B.; Ortiz, J. V.; Cui, Q.; Baboul, A. G.; Clifford, S.; Cioslowski, J.; Stefanov, B. B.; Liu, G.; Liashenko, A.; Piskorz, P.; Komaromi, I.; Martin, R. L.; Fox, D. J.; Keith, T.; Al-Laham, M. A.; Peng, C. Y.; Nanayakkara, A.; Challacombe, M.; Gill, P. M. W.; Johnson, B.; Chen, W.; Wong, M. W.; Gonzalez, C.; and Pople, J. A. *Gaussian 03*, revision C.02; Gaussian, Inc.: Wallingford, CT, 2004.
- (51) Frisch, M. J.; Trucks, G. W.; Schlegel, H. B.; Scuseria, G. E.; Robb, M. A.; Cheeseman, J. R.; Scalmani, G.; Barone, V.; Mennucci, B.; Petersson, G. A.; Nakatsuji, H.; Caricato, M.; Li, X.; Hratchian, H. P.; Izmaylov, A. F.; Bloino, J.; Zheng, G.; Sonnenberg, J. L.; Hada, M.; Ehara, M.; Toyota, K.; Fukuda, R.; Hasegawa, J.; Ishida, M.; Nakajima, T.; Honda, Y.; Kitao, O.; Nakai, H.; Vreven, T.; Montgomery, J. J. A.; Peralta, J. E.; Ogliaro, F.; Bearpark, M.; Heyd, J. J.; Brothers, E.; Kudin, K. N.; Staroverov, V. N.; Kobayashi, R.; Normand, J.; Raghavachari, K.; Rendell, A.; Burant, J. C.; Iyengar, S. S.; Tomasi, J.; Cossi, M.; Rega, N.; Millam, N. J.; Klene, M.; Knox, J. E.; Cross, J. B.; Bakken, V.; Adamo, C.; Jaramillo, J.; Gomperts, R.; Stratmann, R. E.; Yazyev, O.; Austin, A. J.; Cammi, R.; Pomelli, C.; Ochterski, J. W.; Martin, R. L.; Morokuma, K.; Zakrzewski, V. G.; Voth, G. A.; Salvador, P.; Dannenberg, J. J.; Dapprich, S.; Daniels, A. D.; Farkas, Ö.; Foresman, J. B.; Ortiz, J. V.; Cioslowski, J.; Fox, D. J. *Gaussian 09*, revision A.1; Gaussian, Inc.: Wallingford, CT, 2009.
- (52) Zhao, Y.; Truhlar, D. G. The M06 suite of density functionals for main group thermochemistry, thermochemical kinetics, noncovalent interactions, excited states, and transition elements: two new functionals and systematic testing of four M06-class functionals and 12 other functionals. *Theor. Chem. Acc.* **2008**, *120*, 215–241.
- (53) Rydberg, P.; Sigfridsson, E.; Ryde, U. On the role of the axial ligand in heme proteins: a theoretical study. *J. Biol. Inorg. Chem.* **2004**, *9*, 203–223.

- (54) Narasimhulu, S.; Willcox, J. K. Temperature-Jump Relaxation Kinetics of Substrate-Induced Spin-State Transition in Cytochrome P450 (Comparison of the Wild-Type and C334A Mutant P450CAM and P4502B4). *Arch. Biochem. Biophys.* **2001**, *388*, 198–206.
- (55) Mak, P. J.; Denisov, I. G.; Grinkova, Y. V.; Sligar, S. G.; Kincaid, J. R. Defining CYP3A4 Structural Responses to Substrate Binding. Raman Spectroscopic Studies of a Nanodisc-Incorporated Mammalian Cytochrome P450. *J. Am. Chem. Soc.* **2011**, *133*, 1357–1366.
- (56) SMARTS; Daylight Chemical Information Systems, Inc.: Santa Fe, NM; http://www.daylight.com/dayhtml_tutorials/languages/smarts/index.html. Accessed March, 2011.
- (57) Chou, J. T.; Jurs, P. C. Computer-assisted computation of partition coefficients from molecular structures using fragment constants. *J. Chem. Inf. Comput. Sci.* **1979**, *19*, 172–178.
- (58) *clogP*, version 4.71; Daylight Chemical Information Systems, Inc.: Santa Fe, NM.
- (59) Agresti, A.; Coull, B. A. Approximate is better than “exact” for interval estimation of binomial proportions. *The American Statistician* **1998**, *52*, 119–126.
- (60) JMP, version 8; SAS Institute, Inc.: Cary, NC.
- (61) Laurence, C.; Brameld, K. A.; Graton, J.; Le Questel, J.; Renault, E. The pKBHX Database: Toward a Better Understanding of Hydrogen-Bond Basicity for Medicinal Chemists. *J. Med. Chem.* **2009**, *52*, 4073–4086.
- (62) Papadatos, G.; Alkarouri, M.; Gillet, V. J.; Willett, P.; Kadirkamanathan, V.; Luscombe, C. N.; Bravi, G.; Richmond, N. J.; Pickett, S. D.; Hussain, J.; Pritchard, J. M.; Cooper, A. W. J.; MacDonald, S. J. F. Lead Optimization Using Matched Molecular Pairs: Inclusion of Contextual Information for Enhanced Prediction of hERG Inhibition, Solubility, and Lipophilicity. *J. Chem. Inf. Model.* **2010**, *50*, 1872–1886.
- (63) Leach, A. G.; Jones, H. D.; Cosgrove, D. A.; Kenny, P. W.; Ruston, L.; MacFaul, P.; Wood, J. M.; Colclough, N.; Law, B. Matched Molecular Pairs as a Guide in the Optimization of Pharmaceutical Properties; a Study of Aqueous Solubility, Plasma Protein Binding and Oral Exposure. *J. Med. Chem.* **2006**, *49*, 6672–6682.
- (64) Wester, M. R.; Yano, J. K.; Schoch, G. A.; Yang, C.; Griffin, K. J.; Stout, C. D.; Johnson, E. F. The structure of human cytochrome P 450 2C9 complexed with flurbiprofen at 2.0-ANG resolution. *J. Biol. Chem.* **2004**, *279*, 35630–35637.
- (65) Sevirioukova, I. F.; Poulos, T. L. Structure and mechanism of the complex between cytochrome P4503A4 and ritonavir. *Proc. Natl. Acad. Sci. U.S.A.* **2010**, *107*, 18422–18427.
- (66) Beitlich, T.; Kuehnel, K.; Schulze-Briese, C.; Shoeman, R. L.; Schlichting, I. Cryoradiolytic reduction of crystalline heme proteins: analysis by UV-vis spectroscopy and X-ray crystallography. *J. Synchrotron Radiat.* **2007**, *14*, 11–23.
- (67) Kühnel, K.; Derat, E.; Terner, J.; Shaik, S.; Schlichting, I. Structure and quantum chemical characterization of chloroperoxidase compound 0, a common reaction intermediate of diverse heme enzymes. *Proc. Natl. Acad. Sci. U.S.A.* **2007**, *104*, 99–104.
- (68) Rydberg, P.; Olsen, L. The Accuracy of Geometries for Iron Porphyrin Complexes from Density Functional Theory. *J. Phys. Chem. A* **2009**, *113*, 11949–11953.